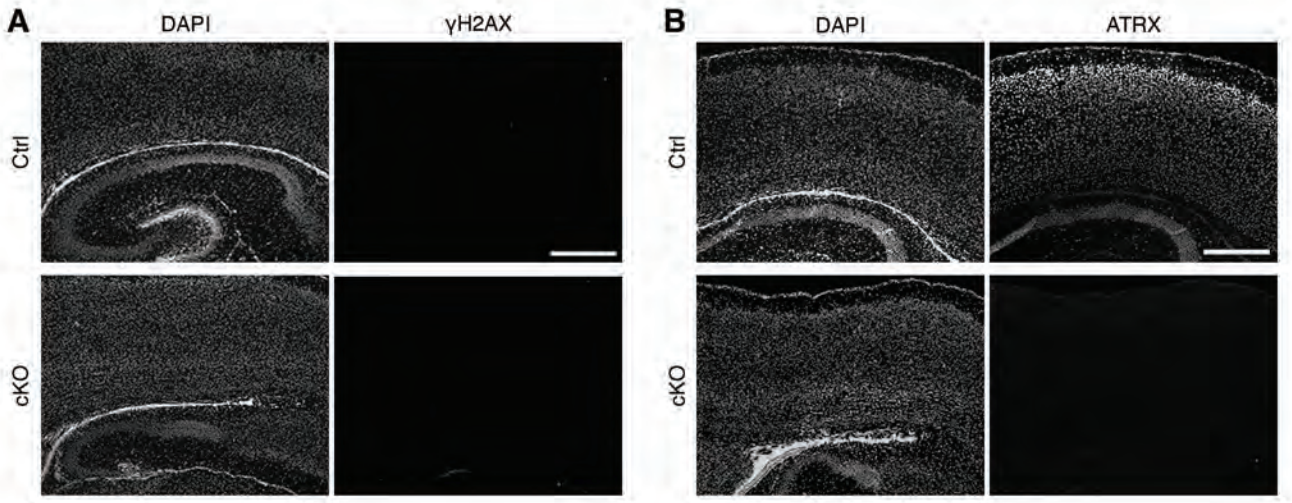

Figure S1

DNA damage is not detected in the ATRX-null postnatal brain. (**A**) Immunostaining for γH2AX in P7 control and cKO cortical cryosections. Scale bar: 200μm. (**B**) Immunostaining for ATRX in P7 control and cKO cortical cryosections. Scale bar: 200μm. Original magnification, x50 (**A** and **B**).

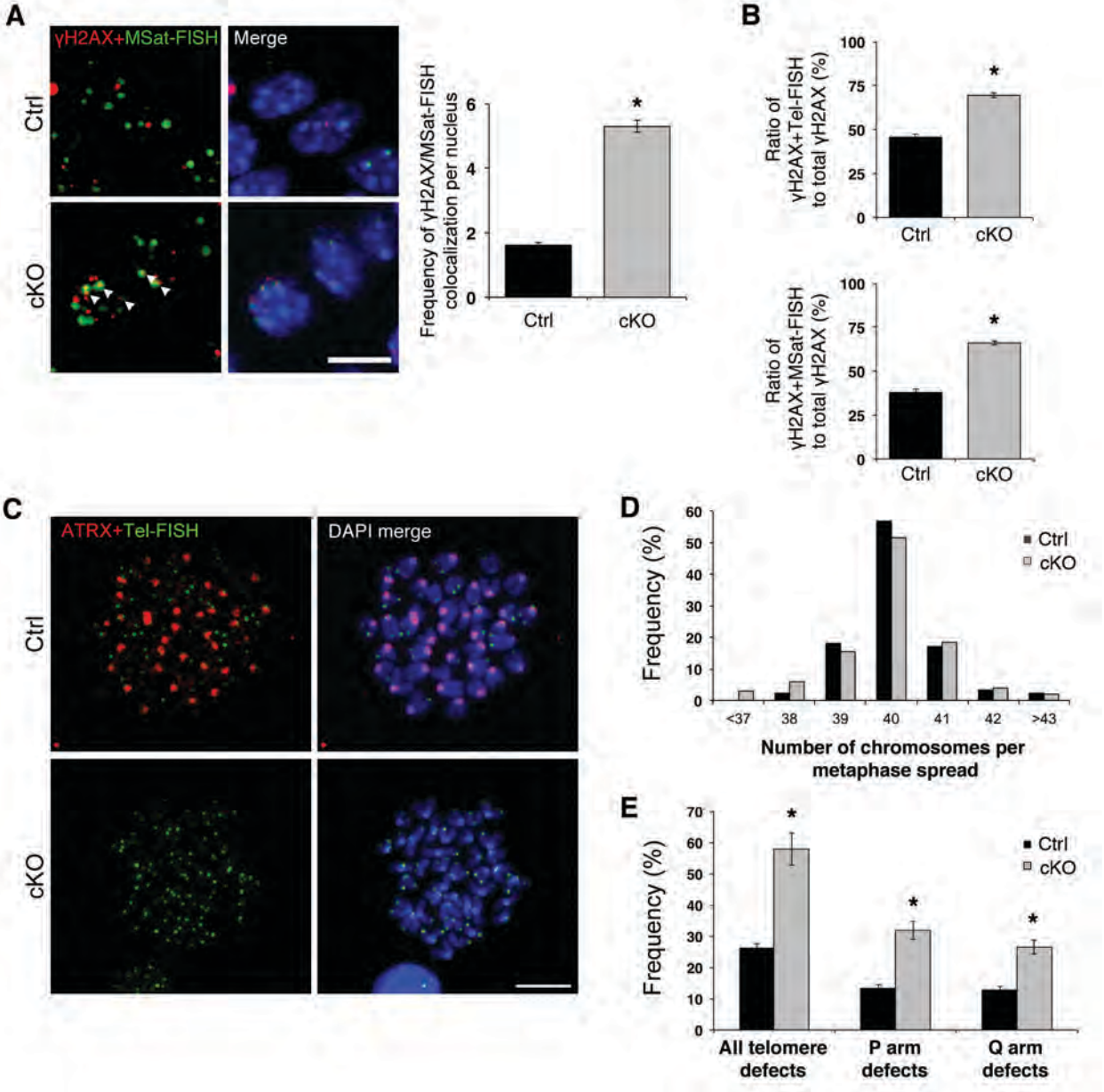

Figure S2

DNA damage occurs at major satellite repeats and telomeric repeats in ATRX-null NPCs, however there is no difference in chromosome number and telomeric defects are not restricted to the p or q arms of cKO chromosomes. (**A**) Confocal immunoFISH images of γH2AX (red) and major satellite repeats (MajSat-FISH; green) shows that DNA damage occurs at PCH more frequently in cKO compared to control NPCs (γH2AX/MSat-FISH colocalization; 300 nuclei counted, $n = 3$). (**B**) Since endogenous γH2AX levels are higher in cKO NPCs compared to control, the ratio of γH2AX and Tel-FISH or MajSat-FISH colocalization vs. total γH2AX foci per cell was calculated to obtain a relative measure of the percentage of γH2AX foci per nucelus that occurred at either telomeres or major satellite repeats (300 nuclei counted, $n = 3$). Scale bar: 10μm. (**C**) ImmunoFISH staining of ATRX (red) and telomeres (Tel-FISH; green) in control and cKO NPCs demonstrates loss of ATRX staining in cKO NPCs. Scale bar: 10μm. (**D**) Chromosome number per metaphase spread did not differ between control and cKO NPCs (control: 88 metaphases and cKO: 108 metaphases, $n = 3$). (**E**) Telomeric defects quantified in Figure 2E were scored for occurring on the P or Q arm of chromosomes. Frequency of defects on either arm did not differ in control and cKO NPCs (1475 chromosomes counted, $n = 3$). Original magnification, x1000 (**A**); x630 (**C**).

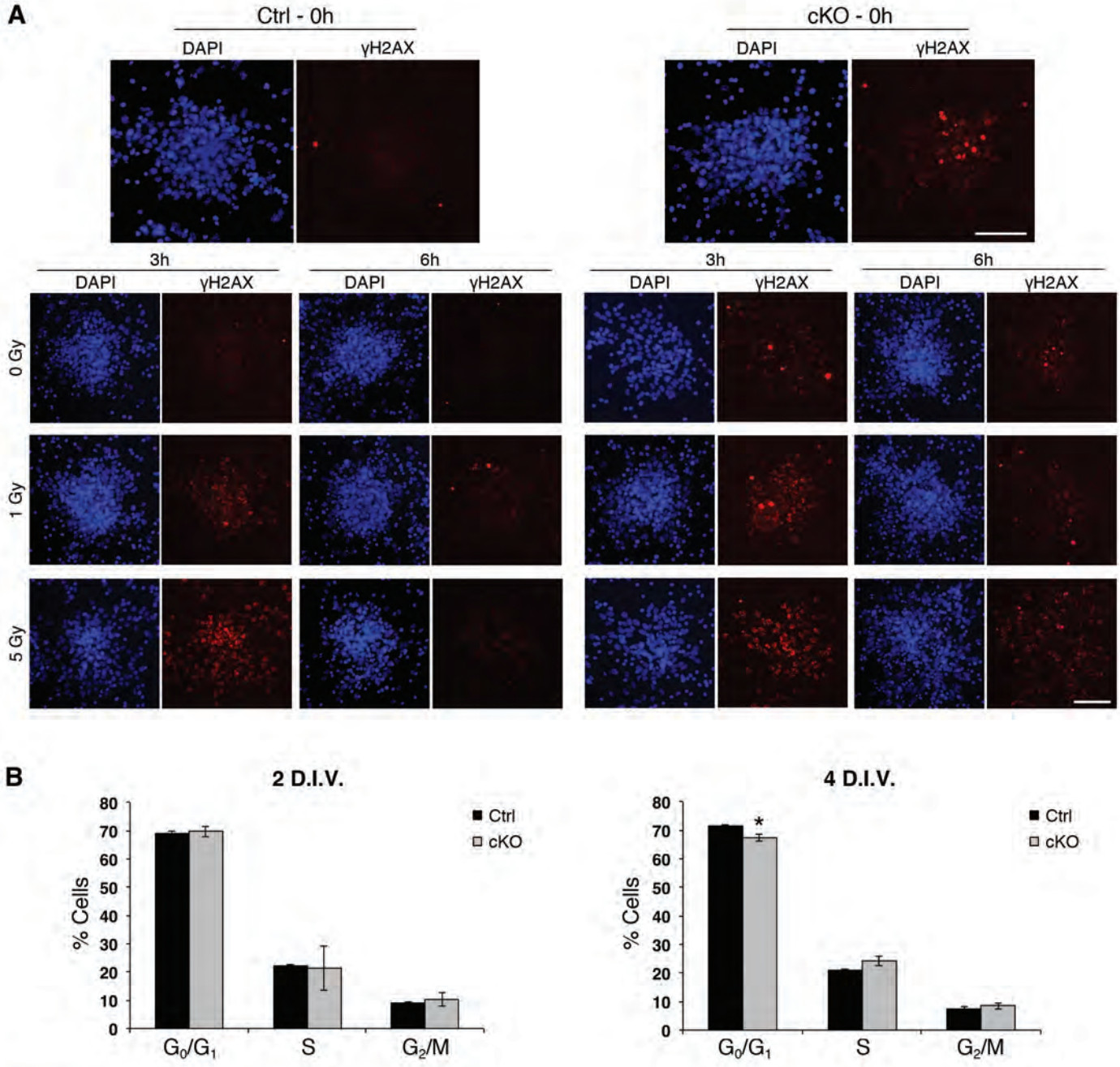

Figure S3

ATRX deficiency does not influence repair of DSBs, however causes a slight decrease in G_0/G_1-phase NPCs with a concomitant increase in S-phase cells at 4 days *in vitro* (D.I.V.). (**A**) Control and cKO NPCs were exposed to 0, 1 and 5 Gy doses of γ-irradiation to induce DSBs. γH2AX signal was assessed at 0h, 3h and 6h post-irradiation. DSBs induced by γ-irradiation were largely repaired by 6h post-treatment in both control and cKO NPCs, as evidenced by the resolution of γH2AX foci. Scale bars: 100μm. (**B**) Actively proliferating control and cKO NPCs were pulse-labeled with BrdU at 2 and 4 D.I.V., processed for flow cytometry, and analyzed for propidium iodide (PI) and BrdU staining. The proportion of cells in each phase of the cell cycle is indicated (n = 3). Original magnification, x200 and x100 (**A**).

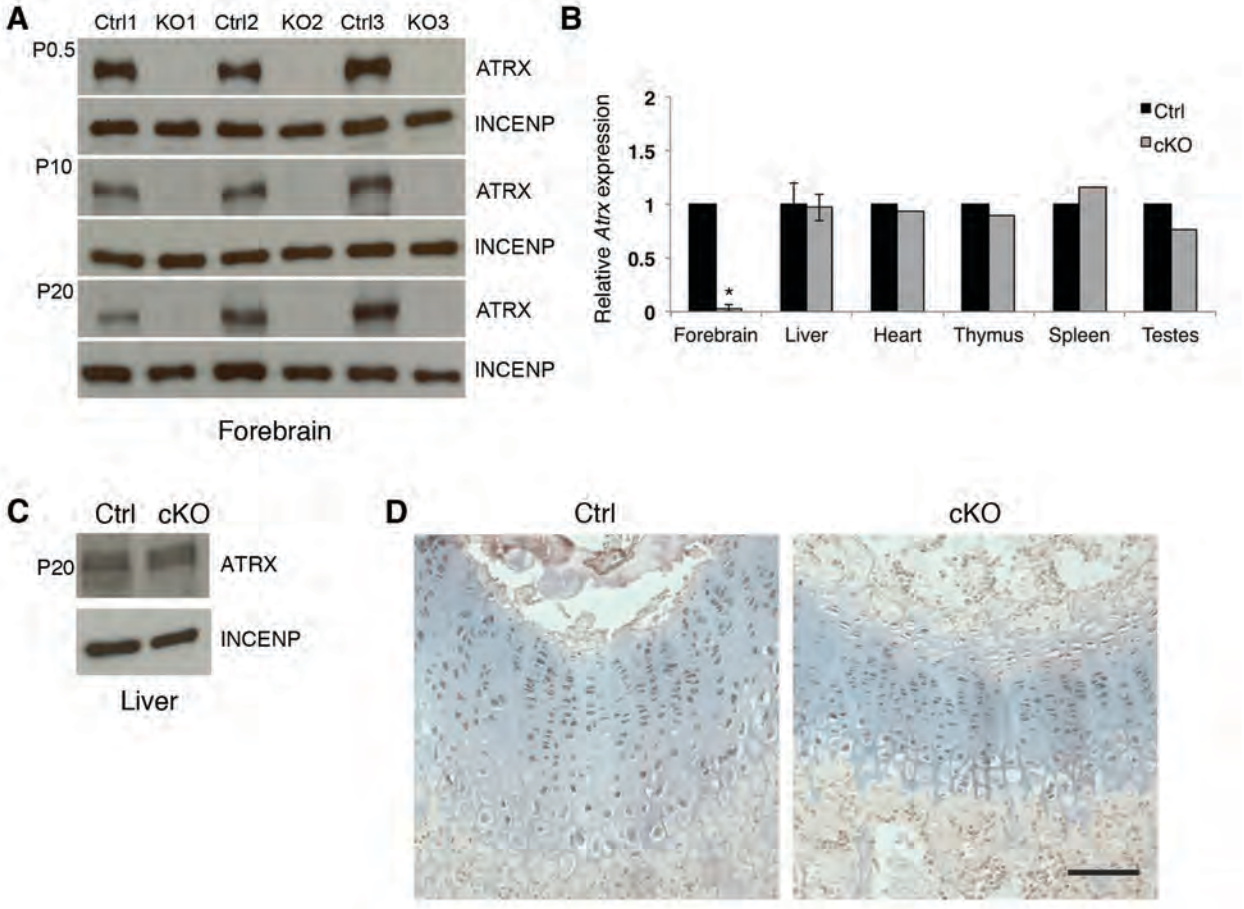

Figure S4

ATRX is specifically deleted in the forebrain. (**A**) Western blot analysis of ATRX expression using nuclear protein extracts obtained from P0.5, P10, and P20 control and cKO telencephalon ($n = 3$). (**B**) Quantitative RT-PCR analysis of *Atrx* expression in P20 control and cKO organs. Forebrain and liver ($n = 3$); heart, thymus, spleen and testes ($n = 1$). Real-time data is normalized to *Gapdh* expression. (**C**) Western blot analysis of ATRX expression using nuclear protein extracts obtained from P20 control and cKO liver. (**D**) Immunohistochemistry detection of ATRX in P20 control and cKO tibia paraffin-embedded sections. Scale bar: 100μm. Original magnification, x50 (**D**).

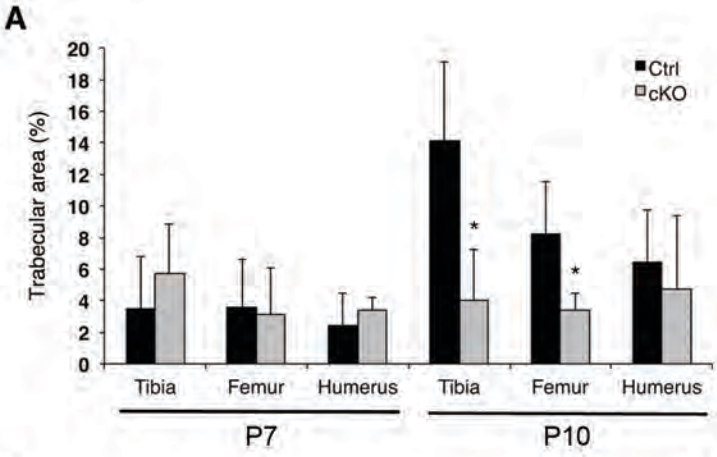

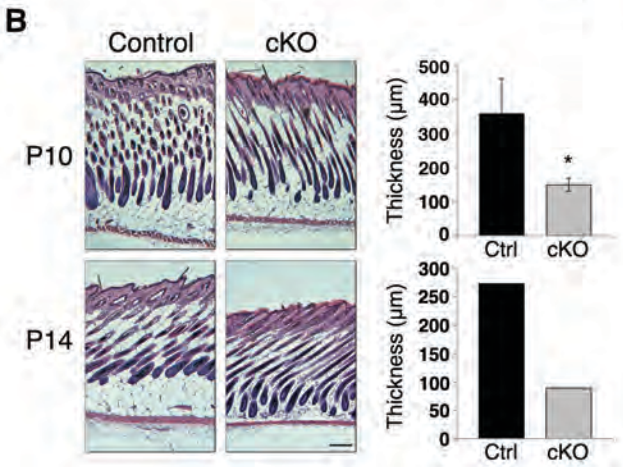

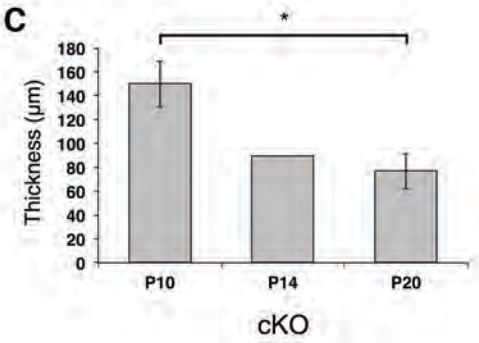

D

	Relative Weight (average g ± SEM)		
	Ctrl	cKO	P value (n)
P10			
Spleen	0.51 ± 0.05	0.40 ± 0.05	0.3354 (3)
Liver	2.49 ± 0.34	1.94 ± 0.07	0.5289 (3)
Kidney	0.63 ± 0.03	0.62 ± 0.04	0.4988 (3)
Thymus	0.46 ± 0.06	0.35 ± 0.04	0.3612 (3)
Heart	0.58 ± 0.03	0.70 ± 0.10	0.0063 (3)
P20			
Spleen	0.39 ± 0.02	0.22 ± 0.02	0.0004 (5)
Liver	3.77 ± 0.14	3.30 ± 0.02	0.0179 (4)
Kidney	0.73 ± 0.04	0.77 ± 0.05	0.5831 (4)
Thymus	0.54 ± 0.04	0.42 ± 0.07	0.1924 (4)
Testes	0.24 ± 0.02	0.28 ± 0.01	0.1090 (3)
Heart	0.58 ± 0.03	0.72 ± 0.05	0.0602 (3)

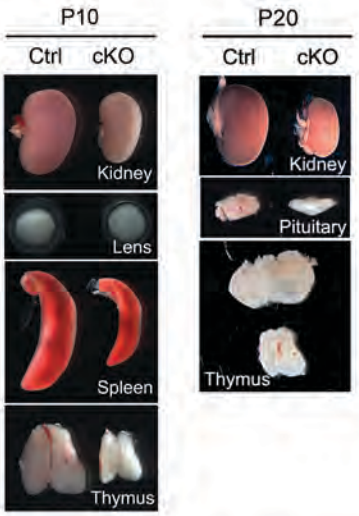

Figure S5

Worsening postnatal phenotypes in ATRX cKO mice. (**A**) Quantification of Picrosirius Red staining in tibia, femur and humerus reveals trabecular bone area is not significantly different between control and cKO until approximately P10 ($n = 3$ at both time points). (**B**) H&E staining of skin cryosections from P10 and P14 shows decreased subcutaneous fat thickness as early as P10 in cKO mice compared to controls (P10, $n = 3$; P14 $n = 1$). Scale bar: 200µm. (**C**) Subcutaneous fat thickness in the *Atrx* cKO at different developmental time points shows cKO mice develop subcutaneous fat (P10), which is gradually reduced in thickness by P20 ($n = 3$ at P10 and P20; $^*P = 0.0409$). (**D**) Organ weight (g) relative to total body weight at P10 and P20. Representative dark field images of organs from control and cKO mice at the indicated time points. Original magnification, x50 (**B**).

Full unedited gel for Figure 1D

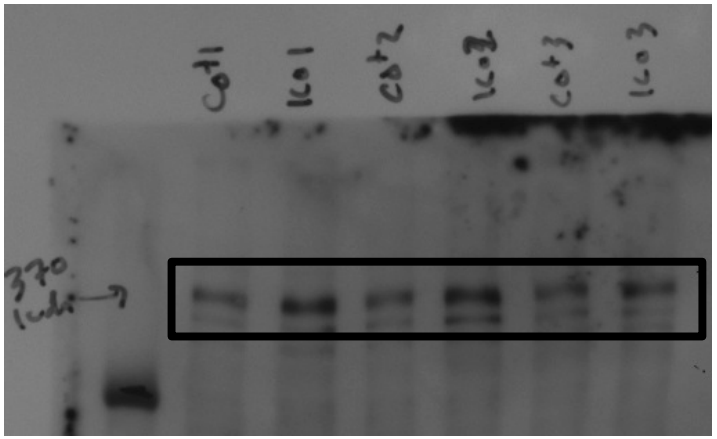

pATM S1981

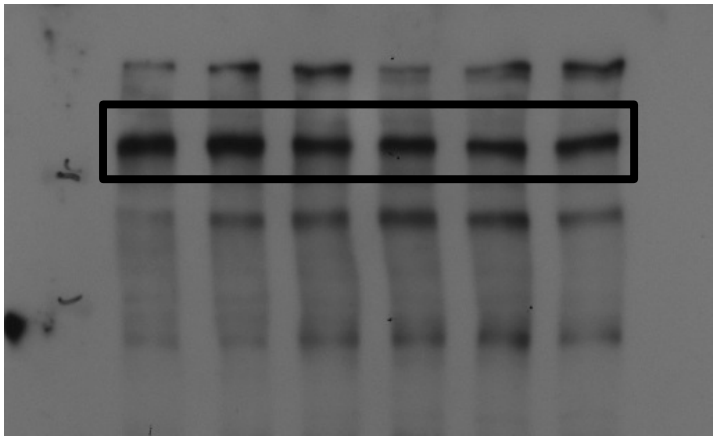

pATR S428

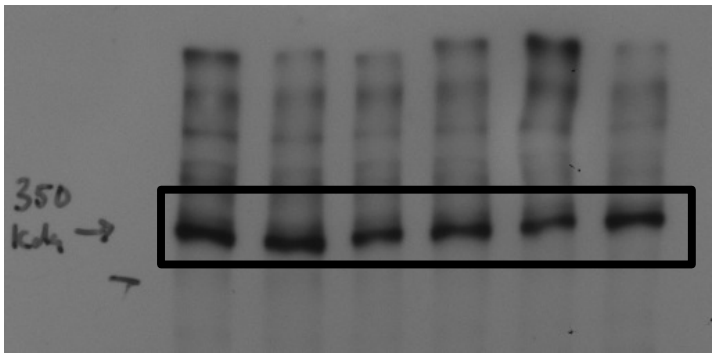

ATM

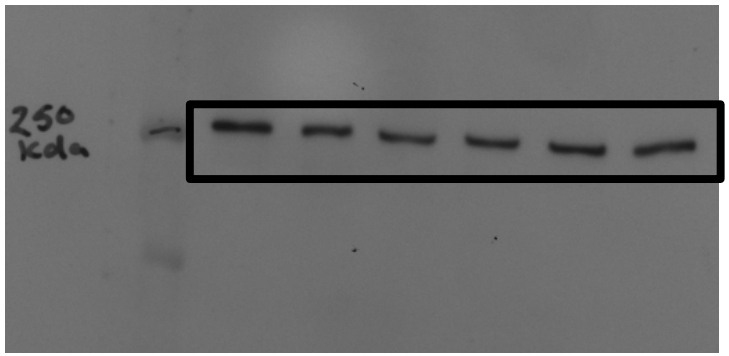

ATR

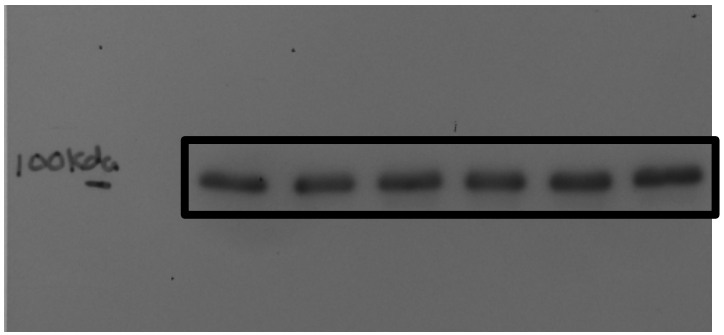

INCENP

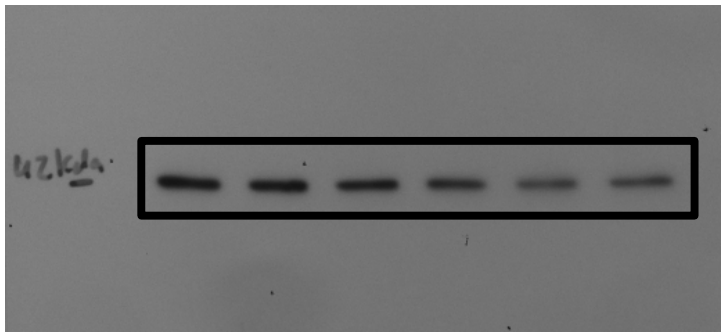

INCENP

Full unedited gel for Figure S4A

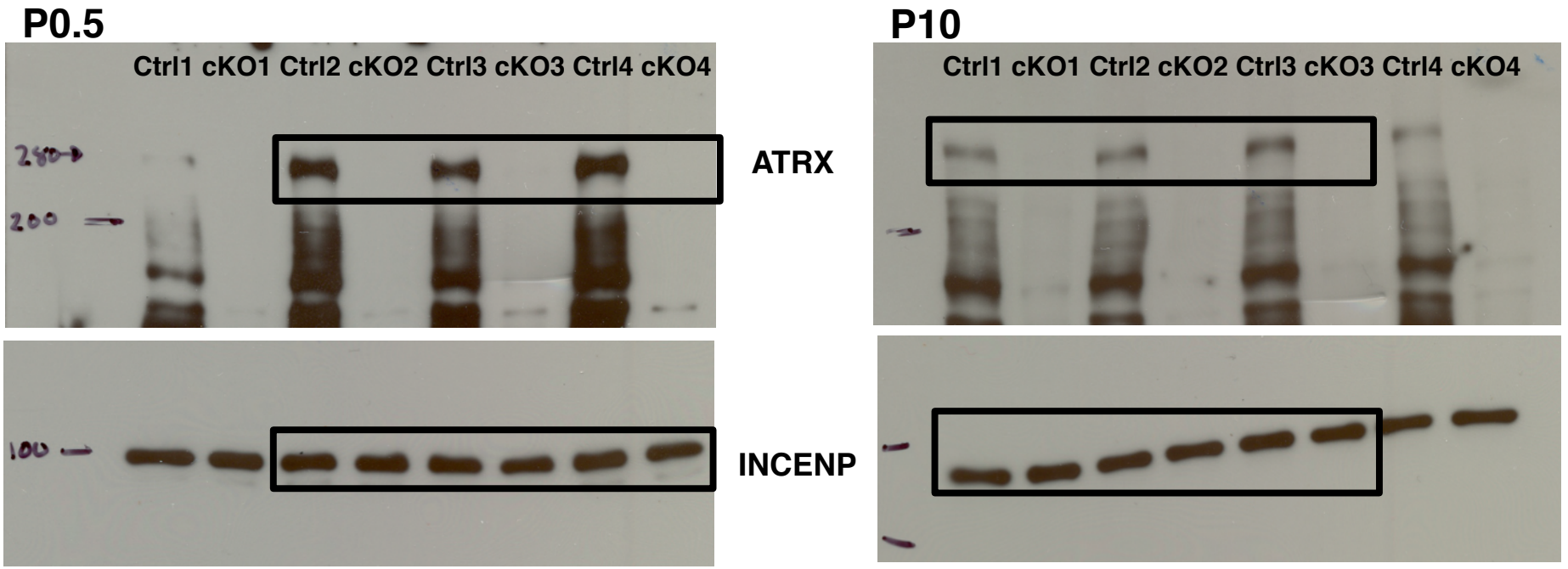

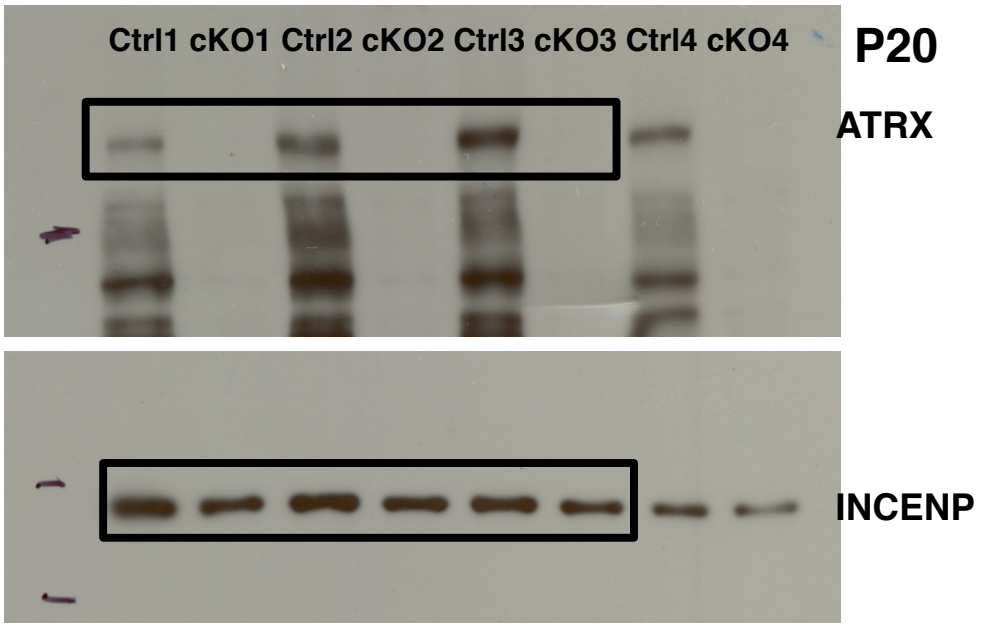

Full unedited gel for Figure S4C